ASTRONOMY & ASTROPHYSICS
SUPPLEMENT SERIES

Astron. Astrophys. Suppl. Ser. **137**, 21–41 (1999)

The ionising cluster of 30 Doradus⋆

II. Spectral classification for 175 stars

G. Bosch[1,⋆⋆], **R. Terlevich**[1,⋆⋆⋆], **J. Melnick**[2], **and F. Selman**[2]

[1] Institute of Astronomy, Madingley Road, Cambridge CB3 0HA, UK
[2] European Southern Observatory, Alonso de Córdova 3107, Santiago, Chile

Received September 16, 1998; accepted February 5, 1999

Abstract. We present spectral types for 175 stars in the ionising cluster of 30 Doradus derived from multislit observations of 231 stars. Comparison with published classifications for 70 stars in common with other authors reveals excellent agreement with the exception of a few cases which are discussed in detail. Our new observations raise to 261 the total number of stars in 30 Dor with known spectral types, outside R136. We analyse the spatial distribution of these stars according to their spectral types, and find evidence for mass segregation.

Key words: stars: Hertzsprung Russell (HR) diagram — stars: luminosity function, mass function — stars: early-type — ISM: dust, extinction — galaxy: open clusters and associations: general — galaxies: Magellanic Clouds

1. Introduction

Starbursts play an important role in the formation and evolution of galaxies (Ellis 1997), and the IMF is the key parameter in starburst models (Stasinska & Leitherer 1996; Elmegreen 1997). One of the few starburst clusters that can be studied in detail (either from the ground or space) is the central cluster of the 30 Doradus giant HII region, which, in fact, has been called the *Rosetta Stone* for young stellar evolution by Walborn (1991).

This paper is the second of a series devoted to the determination of the IMF of the ionising cluster of 30 Doradus. This a-priory simple task is made extremely complex by a number of factors including stellar crowding, strong and variable internal extinction within the cluster, overlapping of stellar ages, and degeneracy of the relation between mass and photometric indices for the most massive stars.

In Paper I of this series (Selman et al. 1999) we combined accurate UBV photometry with spectral classifications in order to determine the extinction law of the dust, and map the distribution of reddening within the cluster. We also introduced a new technique to compare photometry with models in clusters with strong and variable internal extinction.

In this paper (Paper II of the series) we present spectral types for 175 stars in 30 Dor, of which 105 have not been published, obtained with the NTT multi-slit spectrograph. These types were used in Paper I for the study of the extinction law, and will be used in the study of the IMF in Paper III of the series (in preparation). Spectroscopy is critical for the study of the high-mass end of the IMF because it is impossible to determine masses for earliest O-type stars using only photometry (Massey 1985; Massey 1998). In addition to spectral types, the spectroscopy has also been used to determine the radial velocities of the stars. These data will be used in Paper IV of this series (in preparation) to investigate in depth the intriguing possibility of mass segregation in this extremely young cluster which was briefly discussed in Paper I, and which is also discussed in the present paper.

Section 2 describes the spectroscopic observations, Sect. 3 outlines the procedures followed for extracting the spectra, and Sect. 4 shows and discusses the spectral classification itself. The spatial distribution analysis of stars according to their spectral types is presented in Sect. 5.

Send offprint requests to: gbosch@ast.cam.ac.uk

⋆ Based on observations collected at the European Southern Observatory.

⋆⋆ On leave from Facultad de Ciencias Astronómicas y Geofísica, La Plata, Argentina.

⋆⋆⋆ Visiting Professor at I.N.A.O.E., Puebla, Mexico.

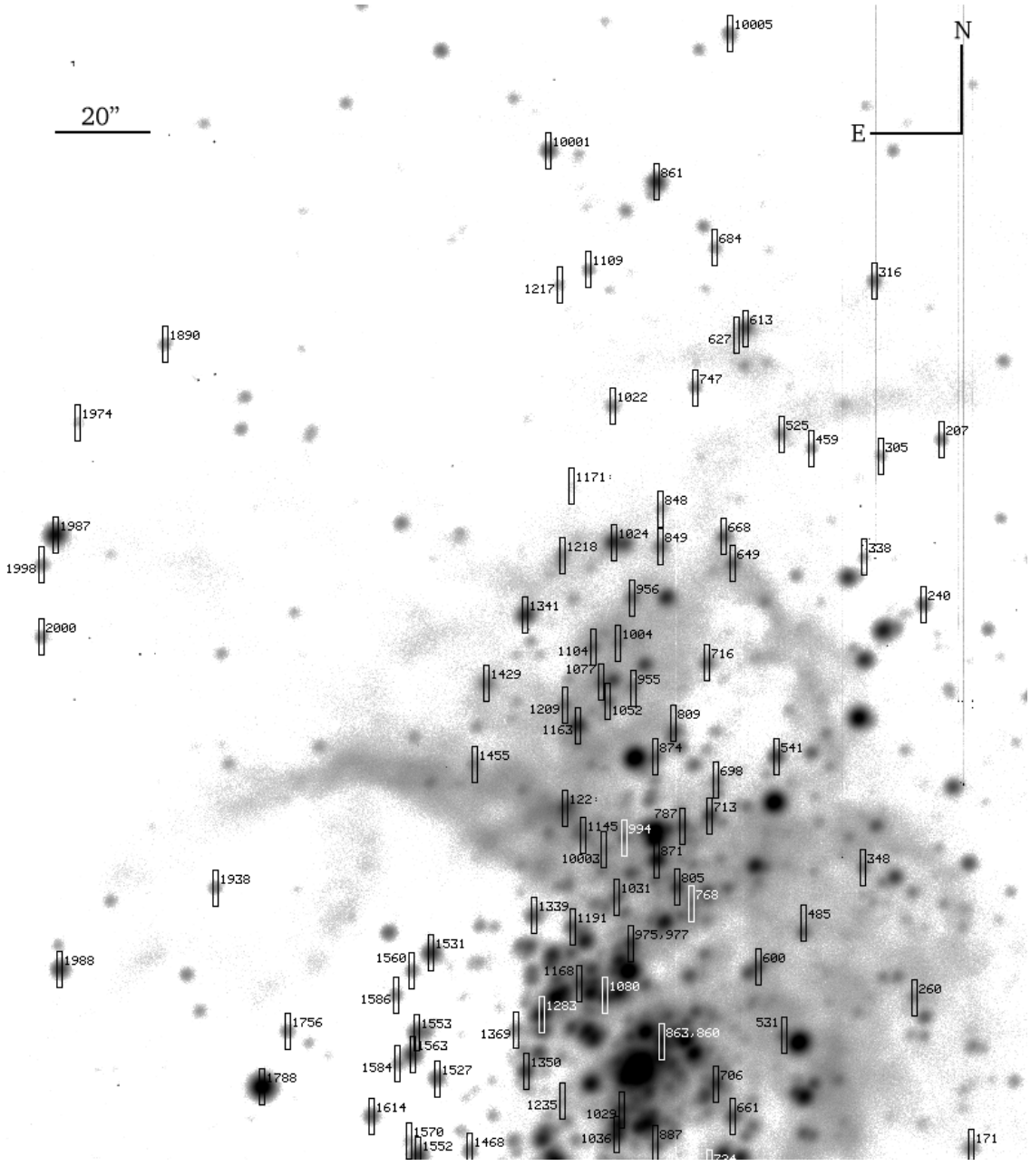

Fig. 1. Finding chart for observed stars north of R136. Stars observed are enclosed by the slit position, drawn to scale. Numbers correspond to the ones listed in Tables 1 and 2. North is to the top, East to the left

2. Observations

The observations were carried out in January 1995, at the ESO 3.5 m NTT using EMMI in its multi-object spectroscopy mode. Grism #5 was employed yielding a dispersion of 1.3 Å/pix on a Tektronix $2048 \times 2048 - 24\,\mu$ pixel CCD detector.

A total of seven starplates were produced using the punching machine mounted inside EMMI from a direct image of the region previously obtained. This provides an excellent accuracy in the slit positions without need for accurate astrometry prior to mask construction. Each starplate contained an average of 30 slitlets thus producing more than 200 spectra in total. The slitlets were 1.1″ wide and 8″ long.

The stars included in each starplate were chosen from the direct images in groups of similar brightness and minimum overlapping. Thus, the number of stars and the exposure times differ from plate to plate. Figures 1 and 2 show

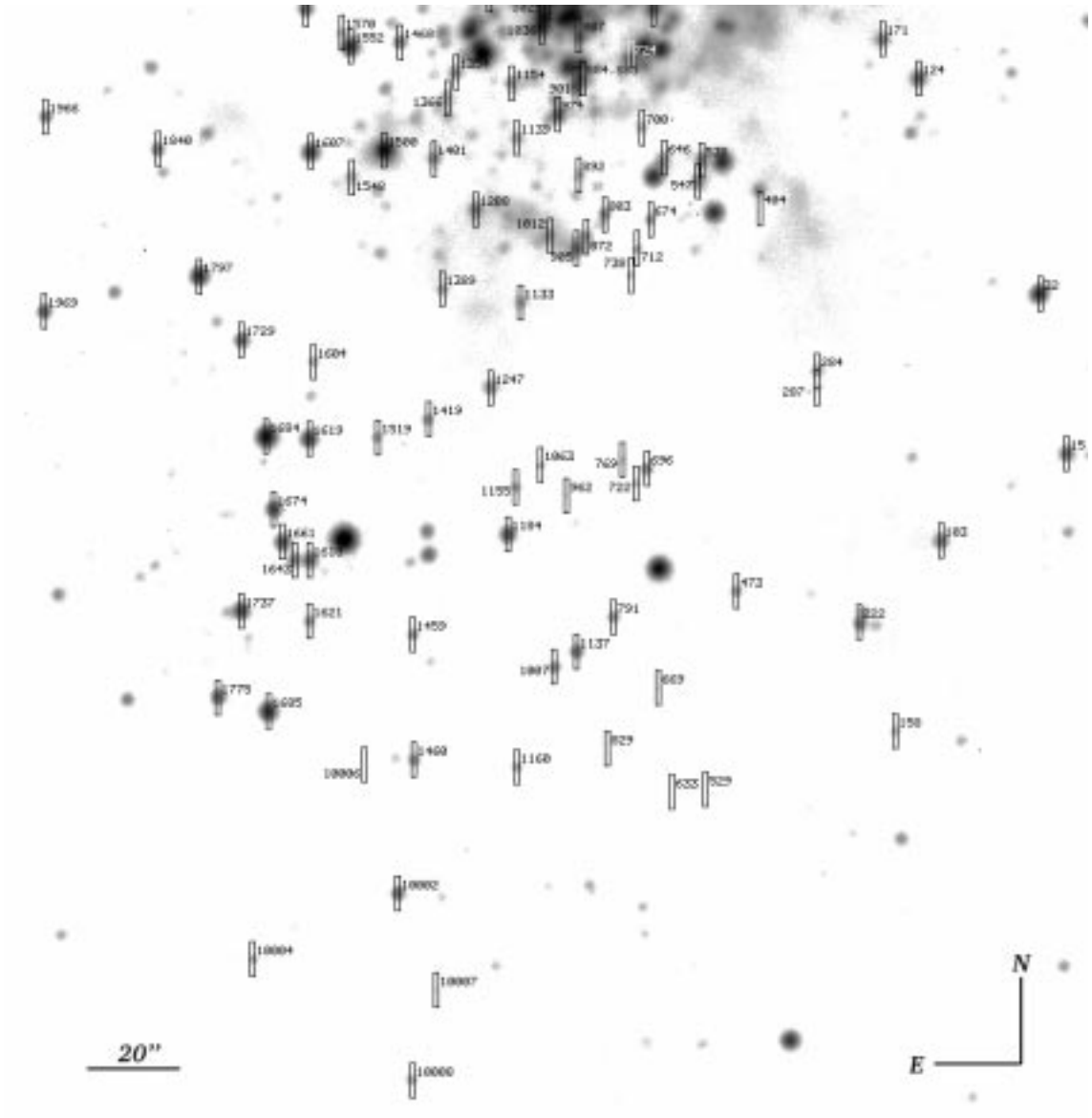

Fig. 2. Same as Fig. 1, for the region south of R136

the slit positions together with the identification numbers from Parker (1993).

He-Ar lamp exposures were taken for wavelength calibration, and halogen lamp exposures were obtained for flat-fielding the images.

3. Reductions

The spectra were reduced using a modified version of the MULTIRED package, which runs within IRAF[1], using the following procedure: (i) for each starplate the location and dimensions of each slit spectrum are determined; (ii) using these parameters, subsections of the image are trimmed to produce individual 2D spectra corresponding to each slitlet; (iii) identical trimming sections are applied to the corresponding bias, flat-field, and wavelength calibration frames; (iv) the bias and flat-field corrections are pipelined in the standard way for the whole set of stellar and arc spectra. This produced 231 individual slit spectra averaging 25 × 1700 pixels each.

3.1. Wavelength calibration

Wavelength calibration was performed on the 2-D images. This is essential in order to correct for possible distortions along the slit, which can prevent a proper nebular background subtraction. He-Ar lines were identified in

[1] IRAF is distributed by the National Optical Astronomy Observatories, operated by the Association of Universities for Research in Astronomy, Inc., under cooperative agreement with the National Science Foundation.

Table 1. Spectral types of the observed stars

Parker id.	$V_{\rm mag}$	Spectral type	Literature Sp. T	Parker id.	$V_{\rm mag}$	Spectral type	Literature Sp. T
15	15.33*	O8.5 V	O9: V [2]	863	13.67	O6.5 V	O3 V [4]
32	14.15*	O9 IV	O8.5 V [2]	871	13.31	O4 V((f*))	O3 V: [1,3]
103	15.56*	B0 V		872	15.98*	O8 V	
122	14.72*	O5-8 V (b)		874	15.70	B2 V	
124	14.96*	O8.5 V	O8-9 III [3]	880	12.66	WN5.5	WN4.5 [1]
158	16.80*	B0.2: III		884	15.28	O6 V	
171	15.82	O8 V	O6-8 Vz [3]	885	14.28	O5 III	
207	15.88*	B1 V		887	15.30	O8 V	
222	15.72*	O9.5-B0 V		892	17.09	B0.5 V	
240	15.48*	O9 V		901	15.11	O3 V((f*))	
260	16.32	B0.5: V		905	15.34*	O9-B0 V	O9-B0 V [3]
284	16.02*	B0.5 III-V		955	15.94*	O9: V	
287	16.61*	B2 V		956	15.58*	B1-2 V	O9-B0 III [3]
305	16.41*	B0-B0.5 V		962	17.17*	B0.5-1.5 V	
316	15.49*	O6.5 V		974	14.76	O5-6 III	O3-6 V [3]
338	16.61*	B0.5-1.5 V		975	14.48	O6-7 V((f))	
348	16.03	B0.2-0.5 V		977	15.31	O6: V	
404	15.75	O4-5 IV-V		994	15.42	B0: V	
459	15.61*	G V		1004	16.21*	B1-2 III-V	
473	16.10*	O5-6 V		1007	15.28*	G V	
485	15.39	O8-9 V	O7-9 V [3]	1012	16.14*	O8-9 V	O7-8 III [3]
525	16.24*	B0-1: I		1013	14.47	O4 V	O8: V [3]
529	17.58*	G V		1022	15.93*	O5: V	
531	15.51	O8 V		1024	13.99*	O9-B0 V (b)	O9:n [3], O [1]
538	15.11	B0.2 III-I	B0-1 III [3]	1029	13.40	WN 4.5-7 + abs	O3If*/WN6-A [3,4]
541	14.69	O7.5 V	O7-8 III [3]	1031	15.41	B0 V	
547	15.65	O6 V	O8-9 V [3]	1036	13.82	O3-4 V((f*)):	O4-5 V: [3], O3III(f*)
574	16.60*	G8 III		1052	15.30*	B0.2 V	O8-9 III [3]
600	15.03	O3-5 V	O3-6 V [3]	1063	16.45*	O6-7 V	
613	15.08*	O8.5 V (b)		1077	15.25*	O7.5: V	
627	17.14*	B0.2 V		1080	13.88	O3-4 V((f))	O3-4 V((f*)) [2] O3 V((f))
633	17.39*	G0: V		1104	15.47*	B0: V	O7-9 V [3]
646	15.37	Gtype		1109	15.87*	O9 V	
649	15.34*	O8-9 V		1133	16.49*	B0: V:	
661	14.84	O5: V	O3-6 V [3]	1137	18.52*	O8-9 II(f)	
668	15.31*	B0.2 V	B0 III [3]	1139	16.59	B0 V	
669	17.05*	O9: V		1145	15.40*	O8 III-II	
674	15.86	O7.5 V		1154	15.91	B0: V	
684	16.38*	B0: I		1155	16.28*	B0.2 III	
696	15.54*	O9 V	O9.7 Ib [3]	1160	16.30*	B1: III:	
698	16.06	B1: III		1163	14.05	O4 If*:	O3 V((f*)) [3]
700	16.37	O7: V((f))		1168	14.95*	O9.5 V	
706	14.59	O6 V	O3 V [3]	1171	17.38*	O8-B1 V:	
712	16.38*	O6 V		1184	14.46*	B1: II-I	B1 Ia [3]
713	14.62	O5 V	O3-6 V [3]	1191	15.11	B0.2-1 III-IV	
716	15.53*	O5.5 III(f)		1209	15.72	O9-B0 V:	
722	16.36*	B0.2 V		1217	16.67*	O9.5-B0.5 V	
724	14.45	O7 III	O6: V: [3]	1218	16.08*	O6: V	
738	16.75*	B2 Ia		1235	16.87	B0 III	
747	15.83*	O6-8 V		1247	15.83*	B0.5 IV	B2-3 III [3]
768	15.69	O9-B0 V		1283	17.65*	O6 V:((f*))	

Table 1. continued

Parker id.	$V_{\rm mag}$	Spectral type	Literature Sp. T	Parker id.	$V_{\rm mag}$	Spectral type	Literature Sp. T
769	17.0⋆3	B0.5-0.7 V		1288	15.56	O8.5 V	O8 V [3]
787	14.96	O9-B0 V		1339	18.46	B0-0.2 IV	
791	15.84⋆	O5 V	O3-5 V [3]	1341	14.01⋆	O3-4 III(f*)	O5 V [3]
803	15.62	O6 V	O3-5 Vz [3]	1350	14.22	O6 III(f*)	O3-6 V: [3], O3 III(f*) [4]
805	14.52	O5-6 V	O4 V [1]	1354	16.72	B0-0.2 III	
809	15.32	O8-9 V		1366	17.04	B1.5 III-I	
829	16.80⋆	K I		1369	15.78	O8.5 V (b)	
848	16.77⋆	O9-B0: V		1389	16.45⋆	B1: V::	
849	15.74⋆	O9-B0 V		1401	15.98	O8 V	
860	14.02	O7: V((f))	O5-7 V [2], O3 V [4]	1419	16.00⋆	B0-0.2 III-I	B1 III [3]
861	16.27	O7: V		1429	15.39⋆	O4-6V	O3-6 V [3]
1455	16.21	B0.2: V		1685	13.80⋆	B0.5-0.7 III-I	B0.5 Ia [3], B1 II [2]
1459	15.92⋆	O9.5 II	O9-B0 II [3]	1729	14.92⋆	B1 II-III	B0.5 III [3]
1460	15.91⋆	B0-2 V		1737	14.29⋆	B1.5 III	B1 Iab [3], B1 Iab [2]
1468	15.55	O9.5 V		1756	15.65⋆	B0.2 V (b)	
1500	13.09	B0.2 III	B0 Ib [3], B0.5 Ia [1]	1775	14.76⋆	A2-3 I	A I [3]
1519	16.22⋆	B0-0.2 V		1788	12.04⋆	WN6	WN6 [1]
1527	14.94	B1 IV	B1 III [3]	1797	13.68⋆	early Be	B3 Ia [3]
1531	14.16	O6 V((f))	O5: V [3]	1840	15.62⋆	B1 V	
1548	17.32⋆	B2 V		1890	15.86⋆	B0.2 V	
1552	13.88	B2 II-III	B2 Ib: [3]	1938	15.77⋆	O7.5 V (b)	
1553	14.70	O7 V	O3-6: V [3], O(7) V [1]	1966	15.67⋆	B0.2 V	O9:: V: [2]
1560	15.71	O8.5 V		1969	14.91⋆	B0.7 IV	O9-B0 III [3]
1563	14.24	O7.5 II-III(f)	O7.5 [3]	1974	16.19⋆	WC 7-9	
1570	16.68⋆	B0-0.2 IV	O9:: V [2]	1987	13.03⋆	B2 I	B1 Ia [1]
1584	16.70	B0-1 V	B0: V: [2]	1988	14.28⋆	B0.5 V (b)	O9 V: [3]
1586	15.92	O9: V	O9 III [2]	1998	15.81⋆	O9.5 III-IV	O8 V [2]
1604	16.34	B1 V		2000	15.67⋆	O6-7 III(f*)	
1607	14.25	O7: If	O6: III: [3], O3 V(f) [1]	10001	...	O4 V	
1614	15.03	O5-6 V((f))		10002	...	O9.5-B0.2 IV-V	
1618	15.03⋆	B0-0.2 III	B0.5 III [3]	10003	...	B1-1.5 V	
1619	14.18⋆	O8 III(f)	O8 Ib(f) [3]	10004	...	B1.5:	
1621	15.97⋆	B0.2-0.5 III	B0.5-1 III [3]	10005	...	B1-1.5 V	
1643	15.51⋆	O5 V	O3-5 Vz [3]	10006	...	G V	
1661	14.46⋆	B1 III	B0.7 Ia [3]	10007	...	G V	
1674	14.39⋆	B1 Ib	B0.5-0.7 I [3]	10008	...	G type	
1684	12.32⋆	G8V (field)	K0 V [1]				

Notes to Table 1: Columns 1 & 5 indicate identifications from Parker (1993), numbers 10001 to 10008 indicate stars not identified before; Columns 2 & 6 show visual magnitudes from Parker (1993), and Selman et al. (1999), marked with a "⋆"; Columns 3 & 7 list our spectral classification. A "(b)" after the spectral type indicates possible spectroscopic binarity according to our spectra; Columns 4 & 8 list previous classification, if any. The references are: Melnick 1985, (2) Parker (1993), (3) WB97, (4) Malumuth & Heap (1994).

a selected column of each slit, the central one in most cases, and were then traced along the direction of the slit. Unfortunately, problems with the arc lamps that occurred during the observing run imply that in some calibration frames the argon lines are not well exposed and the intense HeI 5875 Å line is saturated. Therefore, in order to avoid systematic effects within the whole sample, we used a 5th order Legendre polynomial for all the pixel-wavelength transformations, and we used the same sub-set of He-Ar lines for all spectra. This procedure is not critical for spectral classifications, but is crucial for stellar radial velocities which will be discussed in a forthcoming paper. The mean rms error of the wavelength

Table 2. Spectral types of 30 Dor stars available in the literature

Parker id.	$V_{\rm mag}$	Literature Sp. T	Parker id.	$V_{\rm mag}$	Literature Sp. T
42	12.50*	O8 II [3]	954	11.50	WN4.5 + OB
61	17.40*	B1-2: V: [2]	982	16.00*	O4: V((f)) [2]
75	15.9*3	B1:: V: [2]	987	11.82	B0.5-0.7 I [3]
76	16.74*	O9:: V: [2]	998	12.86*	WN7 + OB [1]
83	15.44*	O9-9.5 V [3]	1018	13.47	O3 If*/WN6-A [3]
169	14.80	O9-B0 III [3]	1035	14.73*	O3-6 V [3]
195	14.88	O9.7 II [3]	1120	13.77	WC5 + O4 (P,M)
246	15.25	B0.5 V [3]	1130	13.36	O7.5 II [3]
288	14.65	O3-6 V [3]	1134	13.43*	WN4.5 [1]
304	14.17*	O8 V [3]	1140	13.57	O(4) [1]
324	15.26	O7-8 V [3]	1150	13.66	O4 III(f) [3]
341	14.40*	O8-9 Vz [3]	1161	15.42	O9.5 V [2]
355	13.07*	WN6 [1]	1170	16.09	O3-6 V [3]
370	14.30*	O4-5: [3]	1222	14.84	O3-6 V [3]
409	15.03	O3-6 V [3]	1253	12.49	BN0.5 Ia [3]
466	15.48	O9 V [3]	1257	12.55	B0 Ia [3]
488	13.02	B0.5-0.7 Ia [3]	1260	13.94	O3 V [3]
493	13.50	BC1 Ia [3]	1267	14.70	O7: V [2]
499	11.74	A0 Ia [1,3]	1306	14.96	O8 III [3]
515	13.76	WN 8 [1]	1311	13.80	O3 III (f*) [3]
548	12.05	B0.7-1.5 I [3]	1312	13.95	O7 V [1,3]
607	13.66	O4 III(f) [3]	1317	14.69	O4 V [3]
615	15.71	O4-6 III(f) [3]	1340	14.94	O7 Vz [3], O9.5: V [2]
621	14.75	O3-6 V [3]	1416	16.55*	B1: V [2]
643	13.60	ON9: I [3]	1423	14.84*	O3-4 III(f) [3]
662	12.67*	BN6 Iap [3]	1445	13.60*	M I [1]
666	13.76	O3 If*/WN7-A [3]	1554	16.50*	O9: III: [2]
691	13.45 *	WN7 [1]	1573	15.45*	O3-6 V: [2]
761	14.82	O3-6 V [3]	1575	12.01*	B9 Ip [3]
767	12.85	O3 If*/WN6-A [3]	1594	15.13	O7 III [2]
786	12.63*	WN7 [1]	1838	15.77*	early O [2]
830	14.16*	O8-9: [3]	1875	15.64*	B0:: V: [2]
841	15.45	O4-6(n)(f)p [3]	1892	15.63*	O8.5 Vz [3]
850	13.76	B0 III [3]	2022	15.39*	B0.5: V [2]
877	12.12	WC5+WN4 [1]	2041	15.13*	O4: V((f)) [2]
909	14.72*	O8-9 III: [3]	2104	15.69*	B0.5: V [2]
917	13.31	WN7-A [1]	2123	12.87*	B8 Ia [2]
922	12.71	O3 If*/WN6-A [3]	2186	13.58*	early K I [2]
925	14.96*	O8 Iaf [3]	2246	14.76*	O4 V [2]
930	13.76	OC9.7 Ib [3]	2252	15.46*	B1.5 Ia [2]
945	11.37*	WN4.5 [1]	2270	15.31*	O7 V [2]
949	13.44	O4 If [1]	2305	15.20*	B1 III [2]
952	11.94	O7 Iafp [3]	2313	15.39*	B0.5: V [2]

Notes to Table 2: Columns 1 & 4 indicate identifications from Parker (1993);
Columns 2 & 5 show visual magnitudes from Selman et al. (1999) and Parker (1993), marked with a "$\star$";
Columns 3 & 6 list previous classification.
The references are: (1) Melnick 1985, (2) Parker (1993), (3) WB97.

calibration for the 13 lines in common to all spectra is 0.06 Å.

Notice that, since the multislit spectrograph yields different wavelength ranges for different slit positions, the reddest line available for wavelength calibration varies from star to star. This, together with the saturation problems of HeI 5875 Å, introduces different limits to the reliable wavelength interval for each object. These limits, however, are beyond the wavelength range used for spectral classification (3800 Å − 4800 Å.)

3.2. Background subtraction

3.2.1. Spectra extractions

EMMI spectra are slightly curved in the spatial direction forming an arc with up to 5 pixels transversal deviation from centre to edge. On top of that, crowding sometimes causes overlapping of information in adjacent spectra. These two effects often left only a few pixels available for background subtraction, so the usual procedure of selecting background strips in the image for subtracting the sky and nebular contamination could not be performed. On the other hand, the strength of the nebular emission lines from the HII region itself makes the background subtraction crucial for the final quality of the reduced data. Therefore, in order to minimise residuals in the nebular subtraction due to the curvature of the spectral lines, we used the IRAF APEXTRACT task to trace the nebular background as close as possible to the stellar spectra. (In order to use this procedure it is essential to eliminate distortions in the slit direction by performing the wavelength calibration in 2-D, as described above.)

Due to the large variations in the intensity of the nebular HeI emission lines within the slit length, we used – whenever possible – two background windows situated symmetrically on both sides of the stellar spectra. Each window was 3 pix-wide and 6 pix (1.7″) away from the aperture centre, and linear interpolation between the two windows was used to determine the background spectrum.

3.2.2. [OIII] scaling factor corrections

We have devised a method to improve the background subtraction which uses the [OIII]$\lambda\lambda$4959, 5007 Å lines to minimise the residual contamination by the nebular lines.

Since the [OIII] lines are not emitted by the stars and are the strongest lines in the nebular spectrum, the presence of residual emission (or "absorption") features of [OIII] in the final stellar spectra is a sensitive indication of under (or over) subtraction of the nebular background. Although, due to the clumpiness of the ionised gas, the intensity of the nebular spectrum can change significantly on very small distance scales, the intensity ratios of the relevant nebular lines are relatively insensitive to density variations and thus remain constant within the slitlets. We have checked for the stability of the line ratios ([OIII]/Hβ, [OIII]/HeI 4471) for the slits with the strongest [OIII] nebular lines. In all cases, the observed ratios changed less than 20%. Therefore, our estimation (and correction where necessary) using the [OIII] residuals also applies to other nebular lines, and in particular to HeI 4471 Å which is critical for spectral classification of O stars.

The correction was estimated as follows:

1. The flux of the residual [OIII] features present in the stellar spectrum (after background subtraction) was measured. ($F([\mathrm{OIII}])_{\mathrm{residual}}$).
2. The flux of the same feature from the nebular spectrum used for background subtraction ($F([\mathrm{OIII}])_{\mathrm{nebular}}$) was also measured.
3. The parameter
$$\Gamma = \frac{F([\mathrm{OIII}])_{\mathrm{residual}}}{F([\mathrm{OIII}])_{\mathrm{nebular}}}$$
which measures ratio of residual to nebular fluxes was calculated for every object.
4. The nebular spectrum was then scaled by a factor $(1+\Gamma)$ and the background subtraction was performed again.

As shown in Fig. 3, this procedure allowed us to achieve excellent subtraction of the nebular lines in most cases. Where this was not possible, the procedure gave us a good estimation of the amount of contamination present. The critical diagnostic for O-type stars is the ratio of HeI 4471 to HeII 4542. As an indicator of the accuracy of the background subtraction for the former line, we used the ratio of the equivalent widths of HeI 4471 to [OIII]5007 in the nebular spectra. For the whole sample, the average ratio is $\sim$0.004, which indicates that only 0.4% of the residual in [OIII]5007 present in the stellar spectrum will be affecting the flux of the HeI 4471 line.

4. Discussion

4.1. Spectral classification

The stellar spectra were normalised and smoothed using a 3 pixel window, and classified following the criteria of Walborn & Fitzpatrick (1990). We obtained thus reliable spectral types for 175 stars. This is fewer than the 231 slit spectra mentioned in Sect. 3 because many stars were observed more than once, while a few were discarded because the signal-to-noise was too low to classify them properly. The method we have used for background subtraction allows us to estimate if the features present in the stellar spectra are undoubtedly of stellar origin.

Figures 4 to 24 show the classified spectra grouped by similar spectral type. The neutral hydrogen lines, together with the nebular lines that showed problems throughout the background subtraction, have been left out of scale

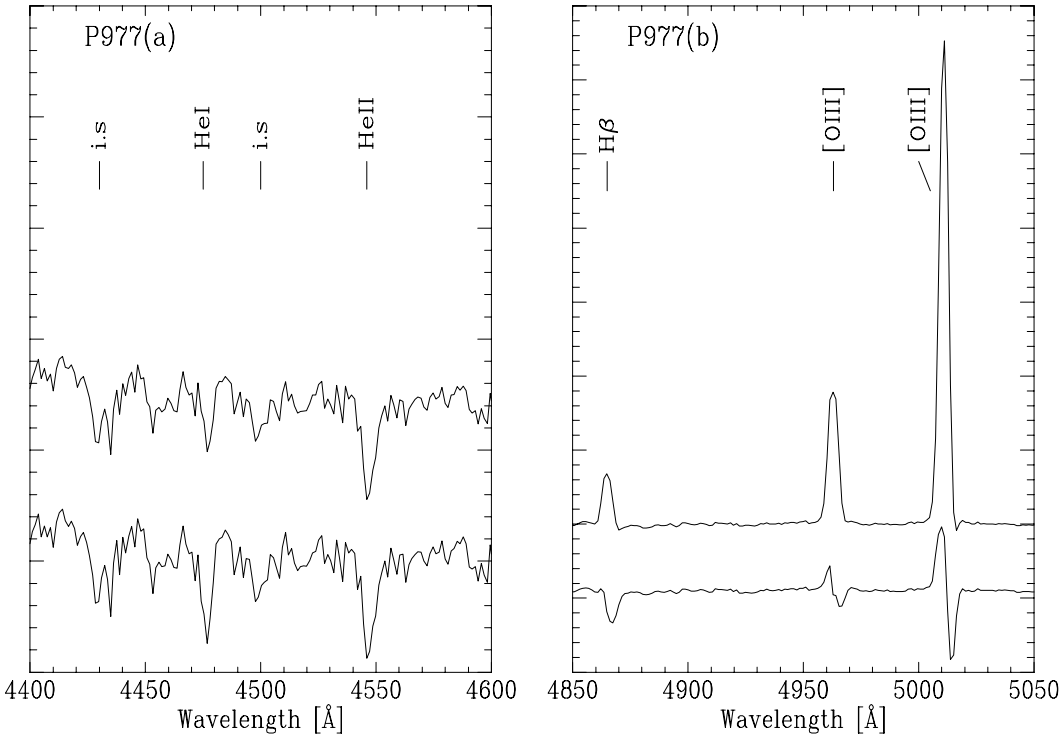

Fig. 3. Both panels show, at different wavelengths, the reduction of the nebular residual with the procedure described in the text, for the case of star 977. Within each panel both spectra, the corrected one being plotted below, are drawn at the same scale. The correction introduced from the [OIII] lines is shown in the right panel. The effects of improved background subtraction can be seen in the left panel, as the observed intensity of the HeI 4471 Å absorption changes

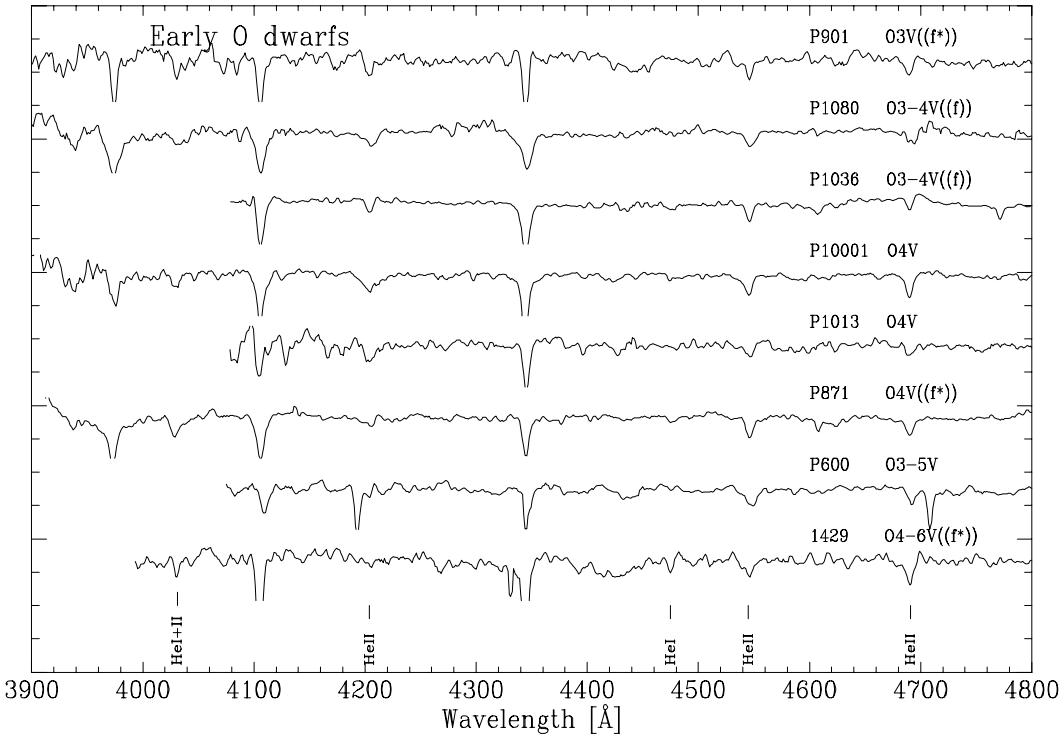

Fig. 4. Spectral classification for early O-type dwarf stars. HeII and HeI lines have been identified as a reference. The range suitable for classification is shown in this figure. The y axis scale is in arbitrary units, each spectrum being normalised to its continuum

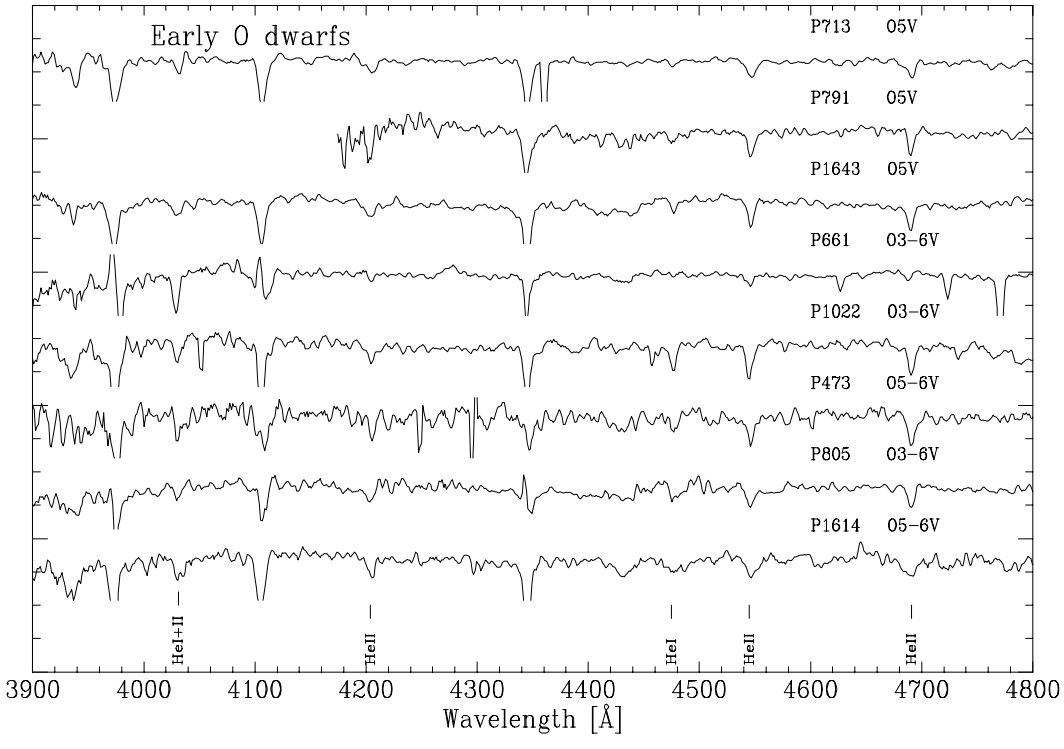

Fig. 5. Same as Fig. 4, stars classified as O3-6 are early O stars, with strong nebular contamination on HeI 4471 Å that prevents from the determination of a more accurate spectral type

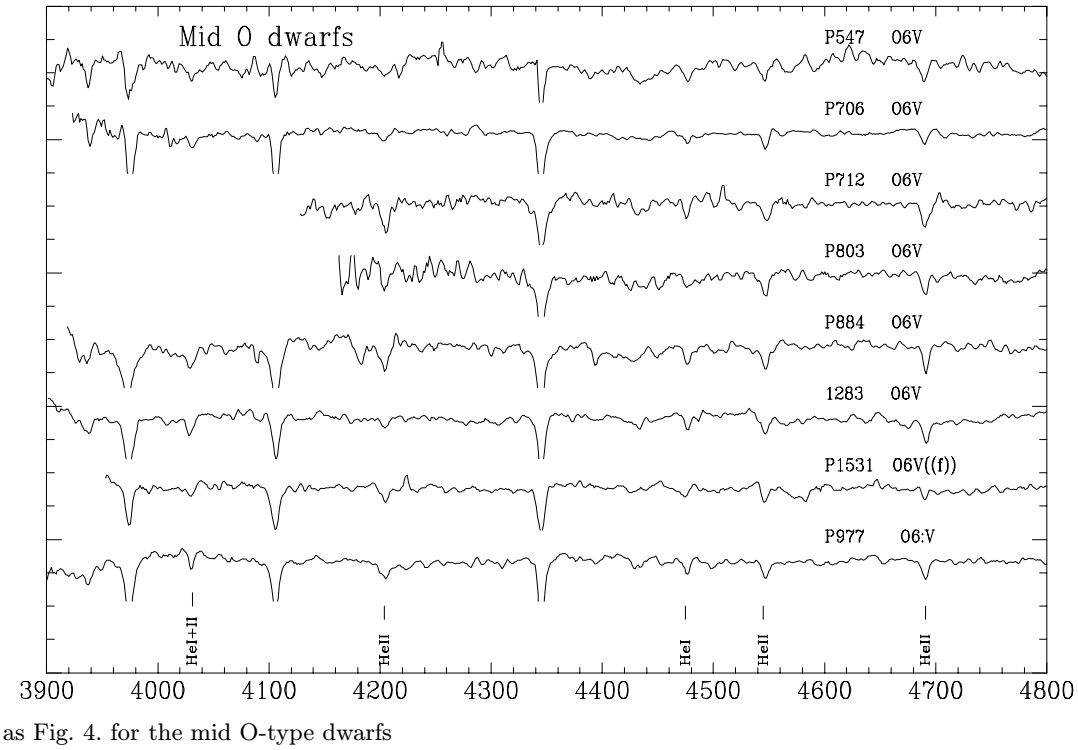

Fig. 6. Same as Fig. 4. for the mid O-type dwarfs

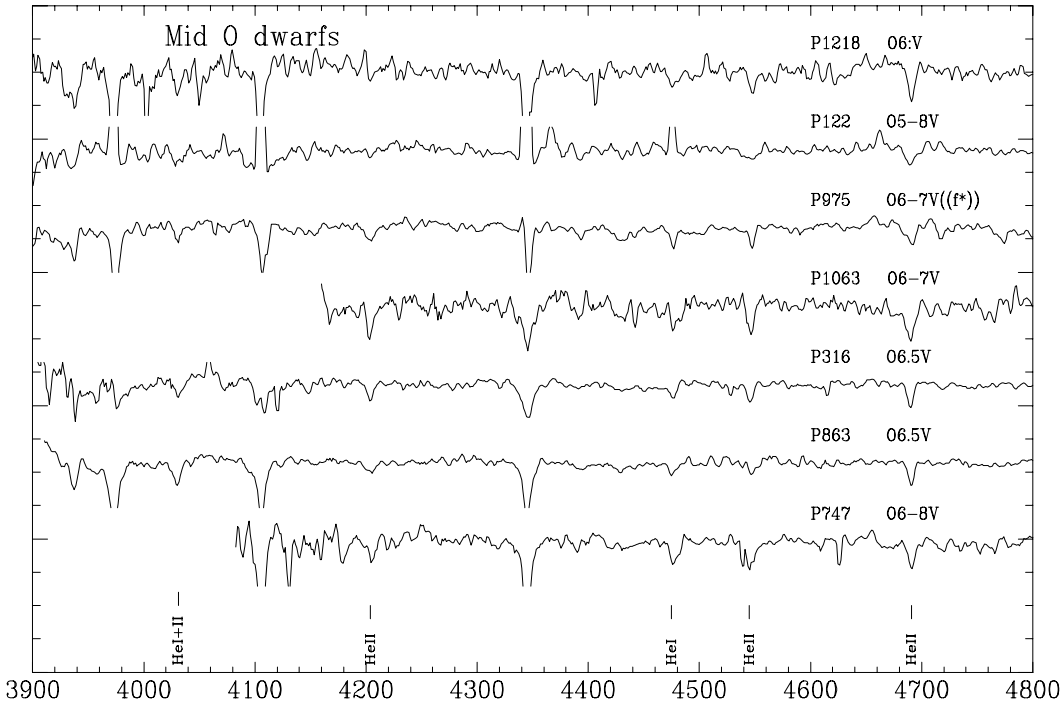

Fig. 7. Same as Fig. 4 for mid-O stars. The O6-8 type indicates weak HeII absorption lines, but with nebular contamination on HeI 4471 Å

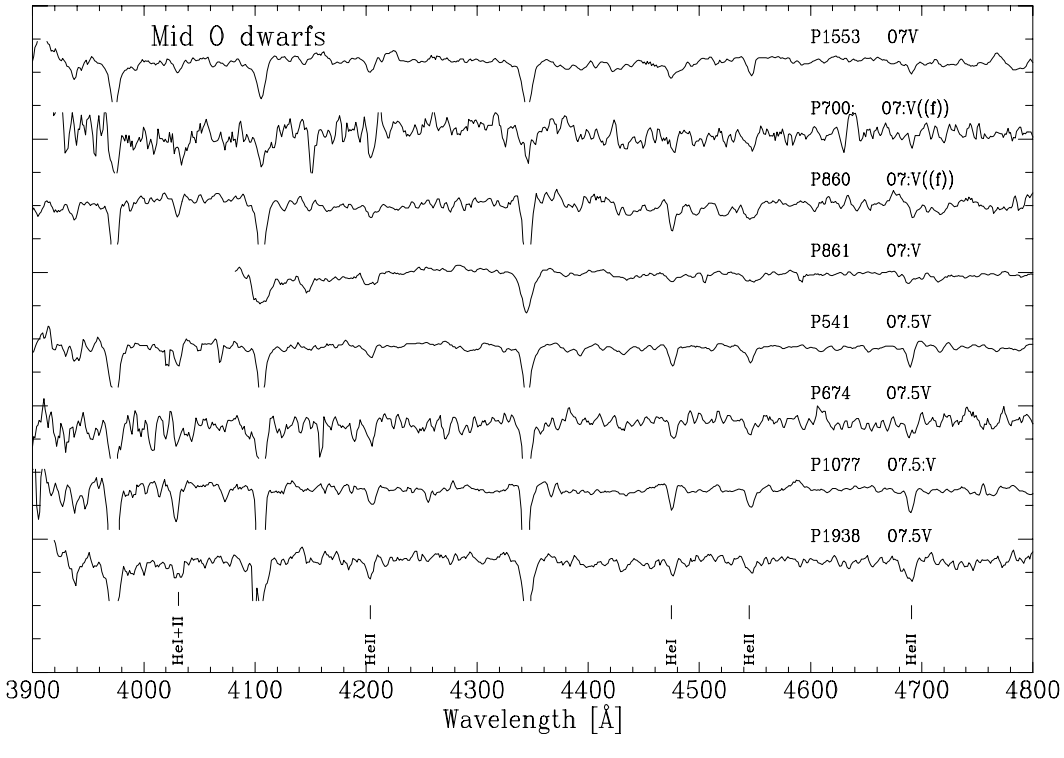

Fig. 8. Same as Fig. 7

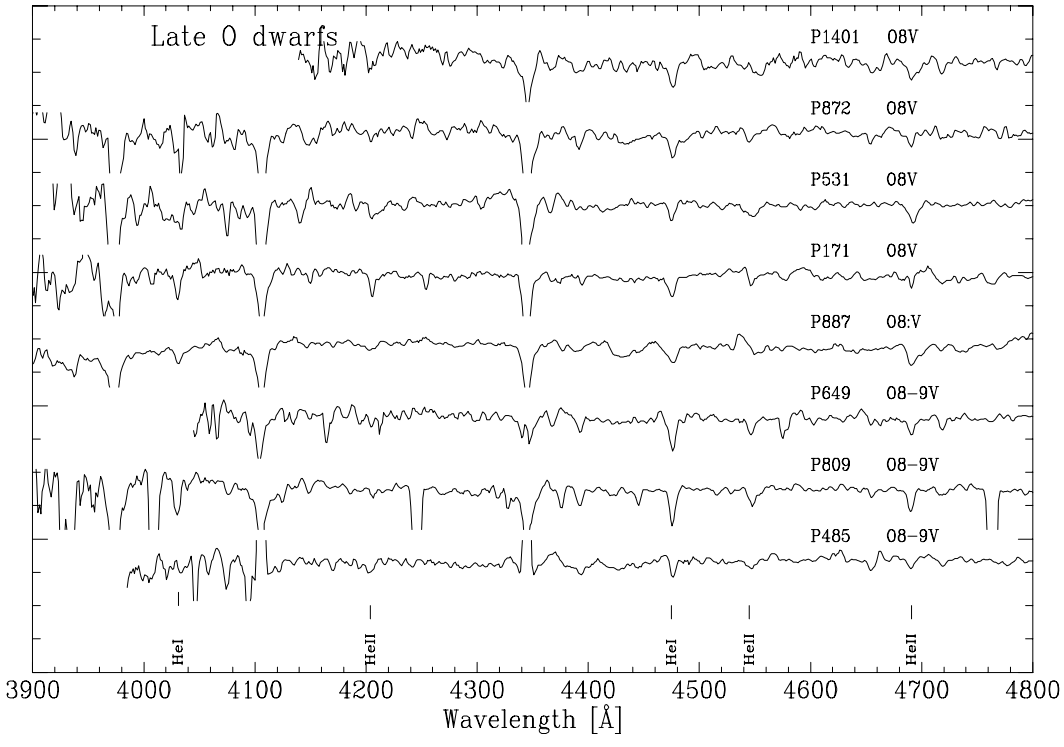

Fig. 9. Same as Fig. 4 for late O-type dwarf stars. As the intensity of the HeII absorption lines diminishes, the feature identified at 4026 Å is only due to HeI

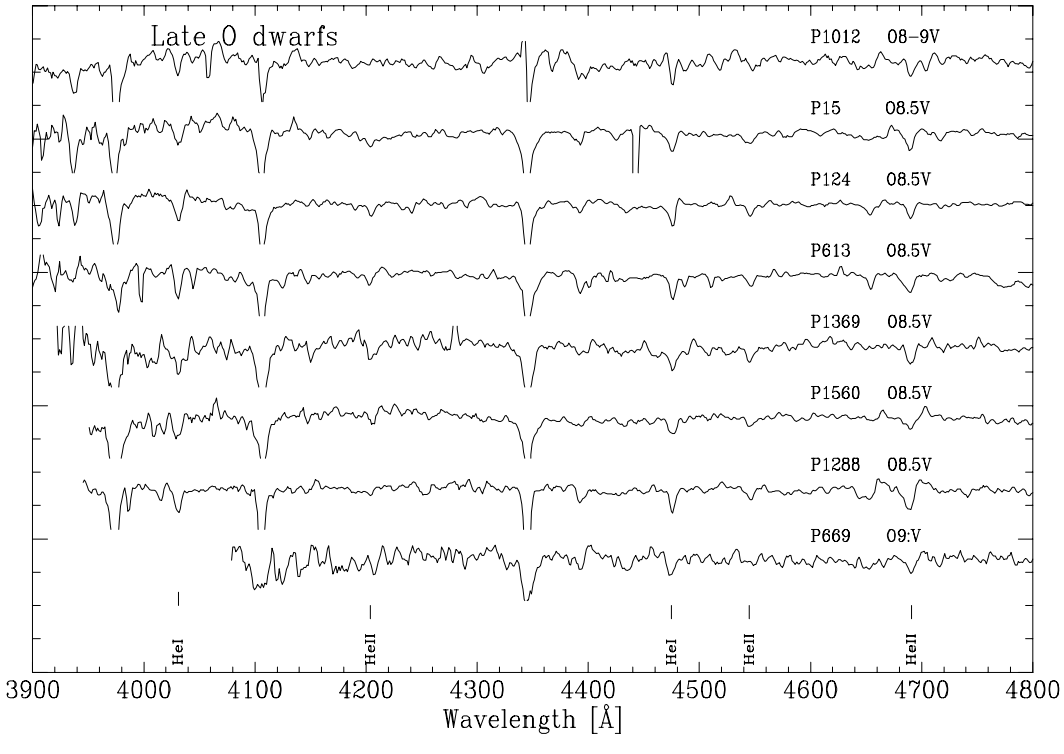

Fig. 10. Same as Fig. 9

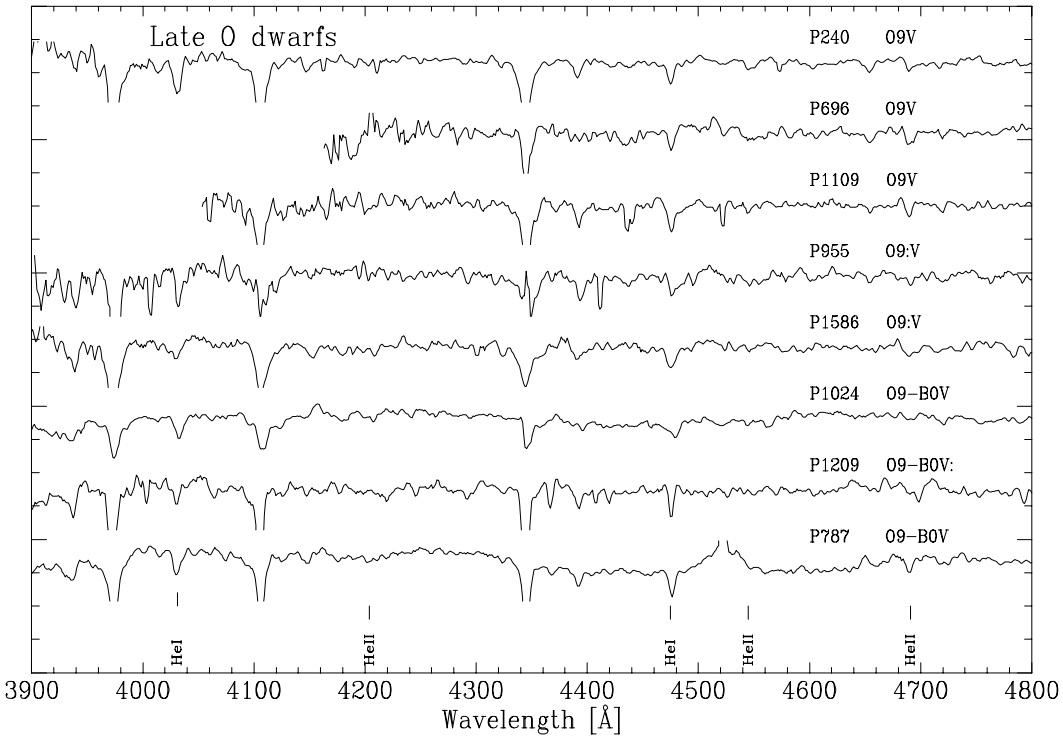

Fig. 11. Same as Fig. 9

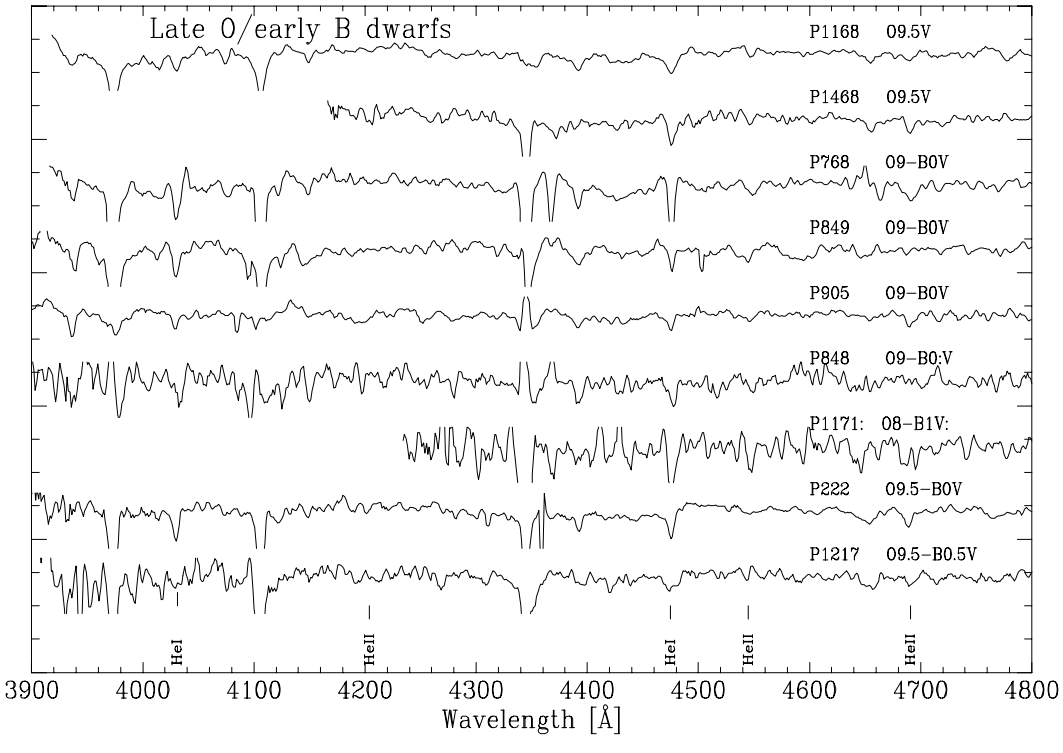

Fig. 12. Same as Fig. 9

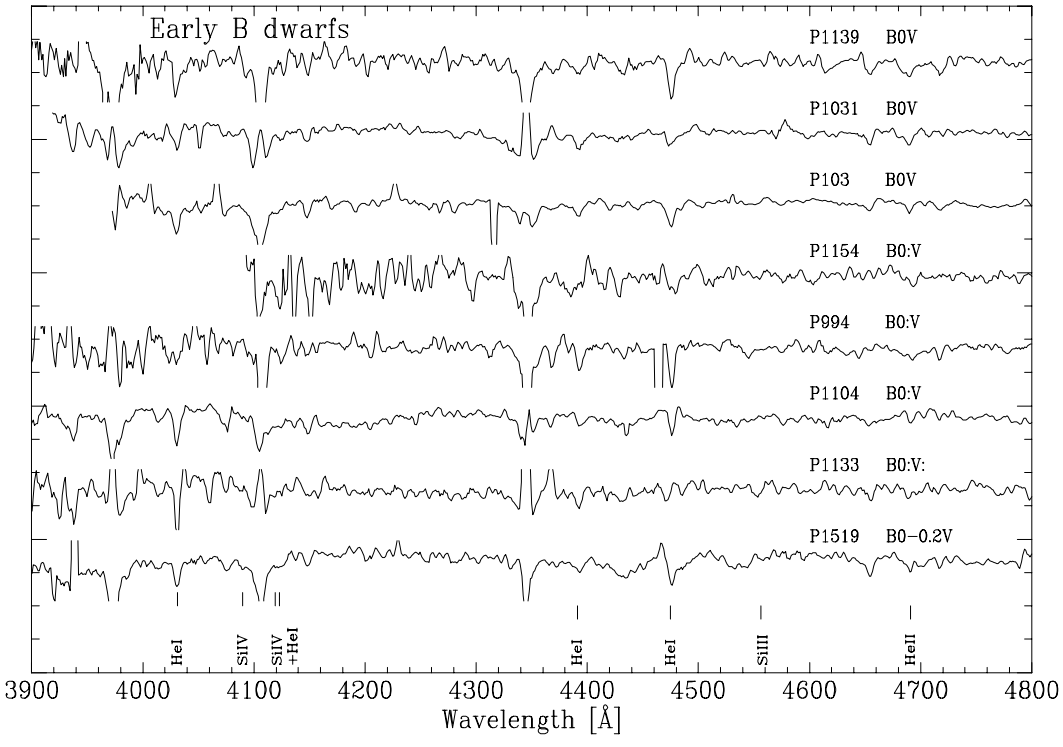

Fig. 13. Same as Fig. 4 for the early B-type dwarfs. Only traces of HeII are detected. SiIII and SiIV, used for classification, are identified here

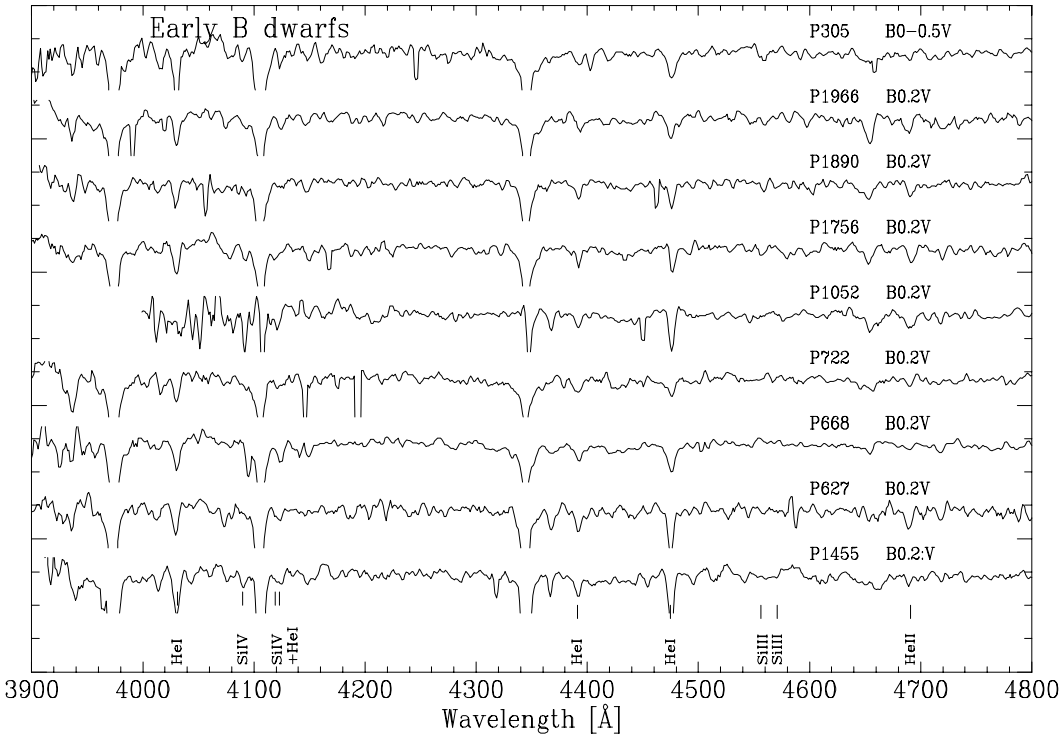

Fig. 14. Same as Fig. 13

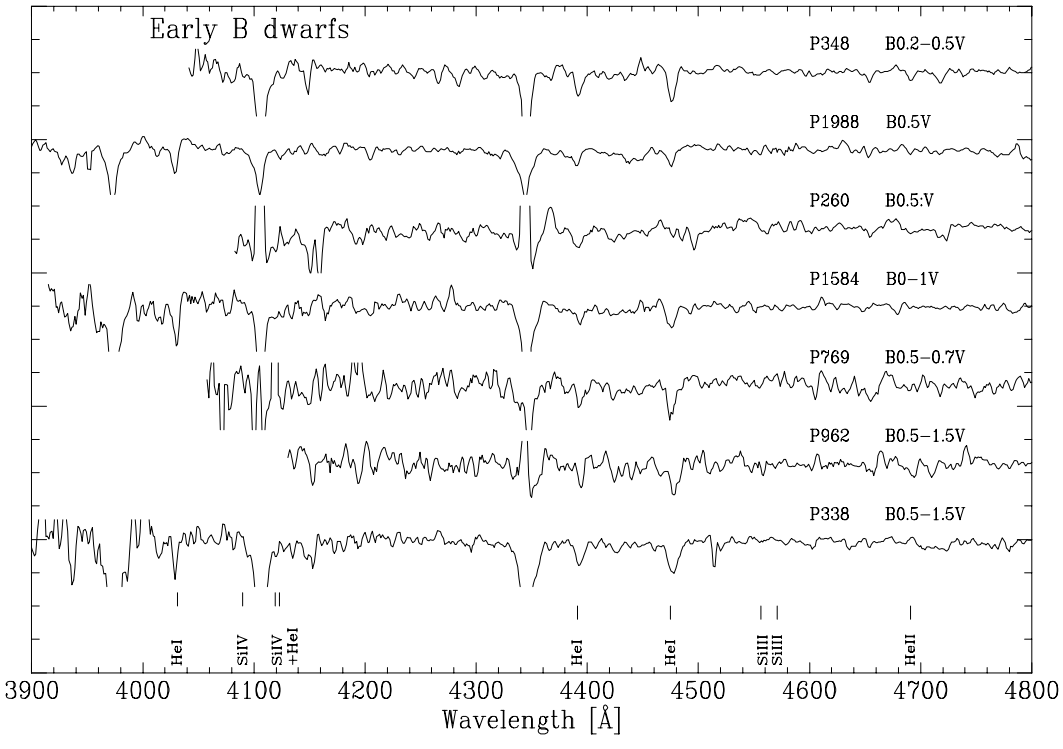

Fig. 15. Same as Fig. 13

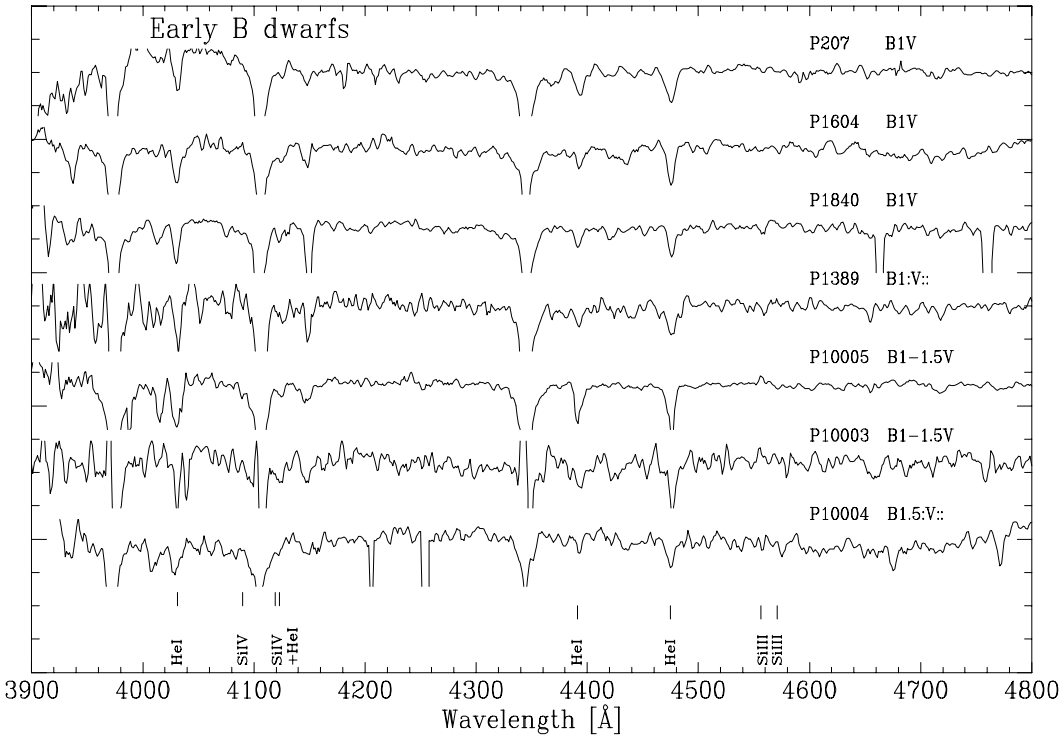

Fig. 16. Same as Fig. 13

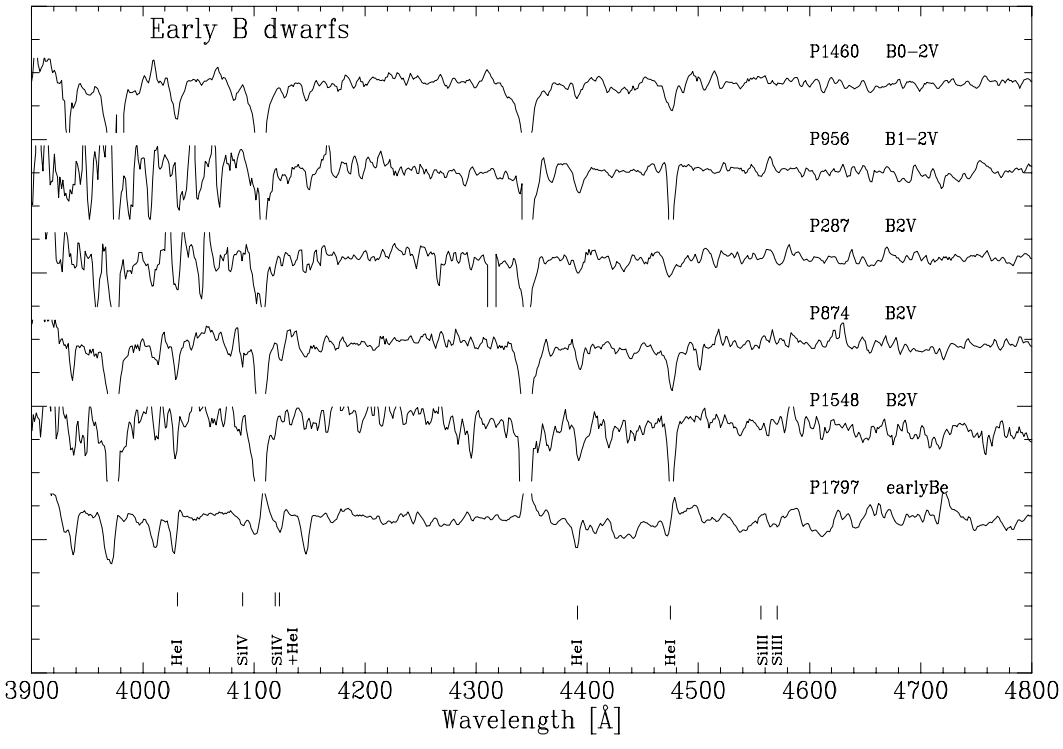

Fig. 17. Same as Fig. 13

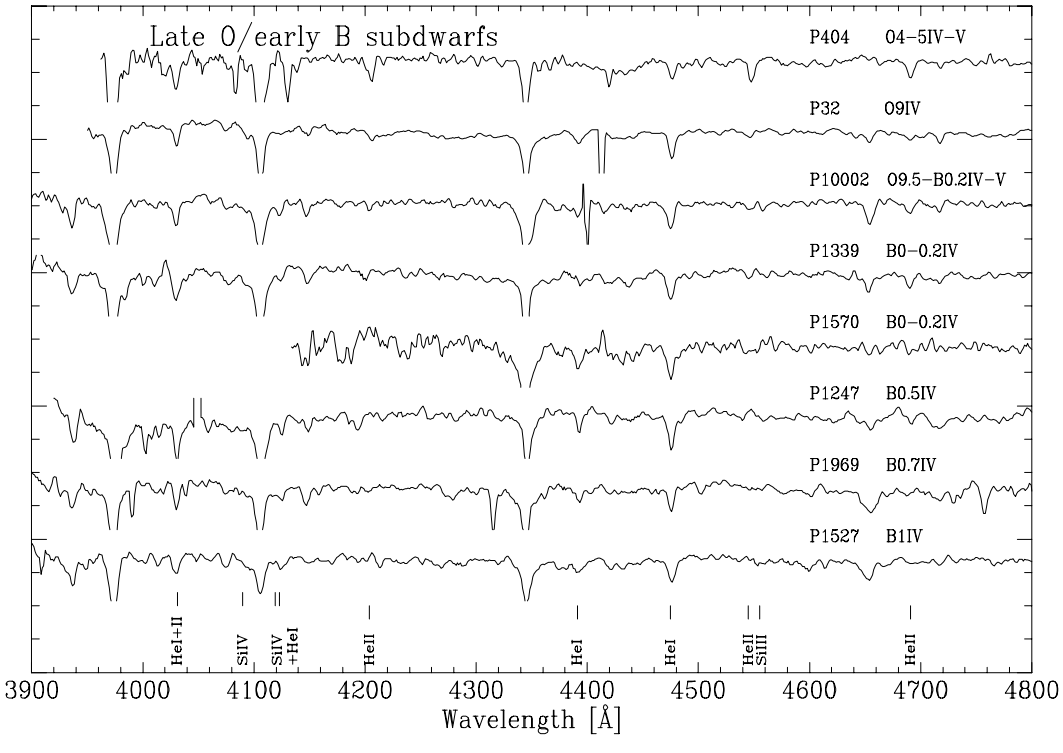

Fig. 18. Same as Fig. 4 for OB-type subdwarf stars

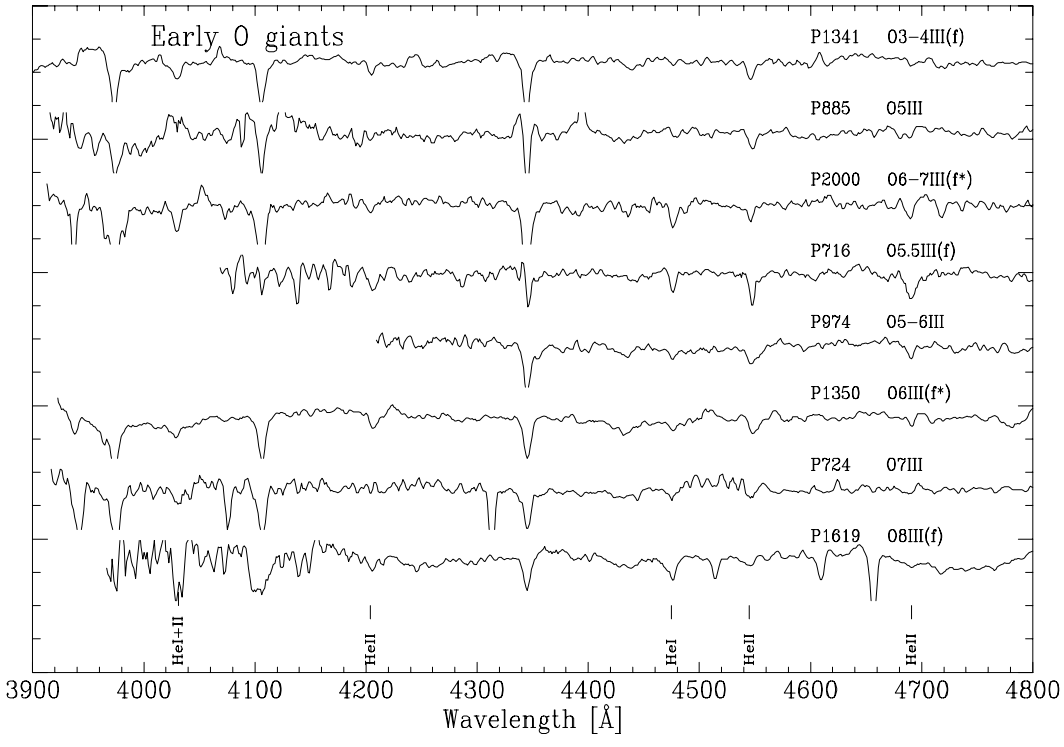

Fig. 19. Spectral classification for early O-type giant stars. HeI and HeII features are identified. The luminosity criterium used is the partial filling of the HeII 4686 Å feature

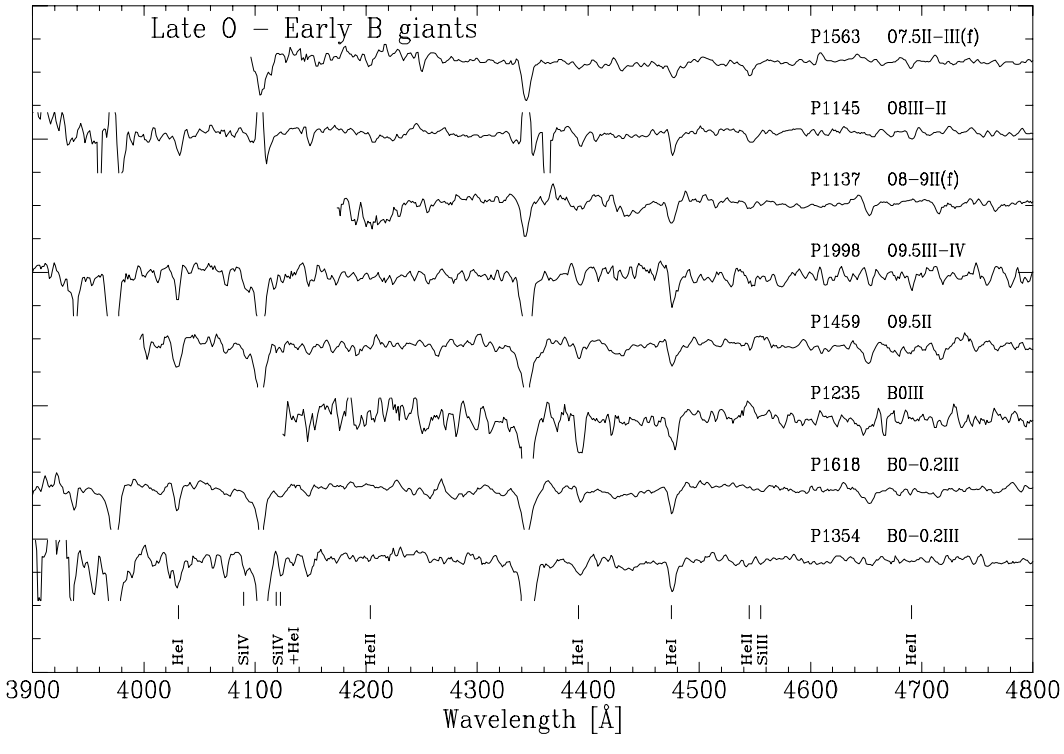

Fig. 20. Same as Fig. 19 for late O - early B type giant stars. Together with HeI and HeII, SiIII and SiIV features are identified

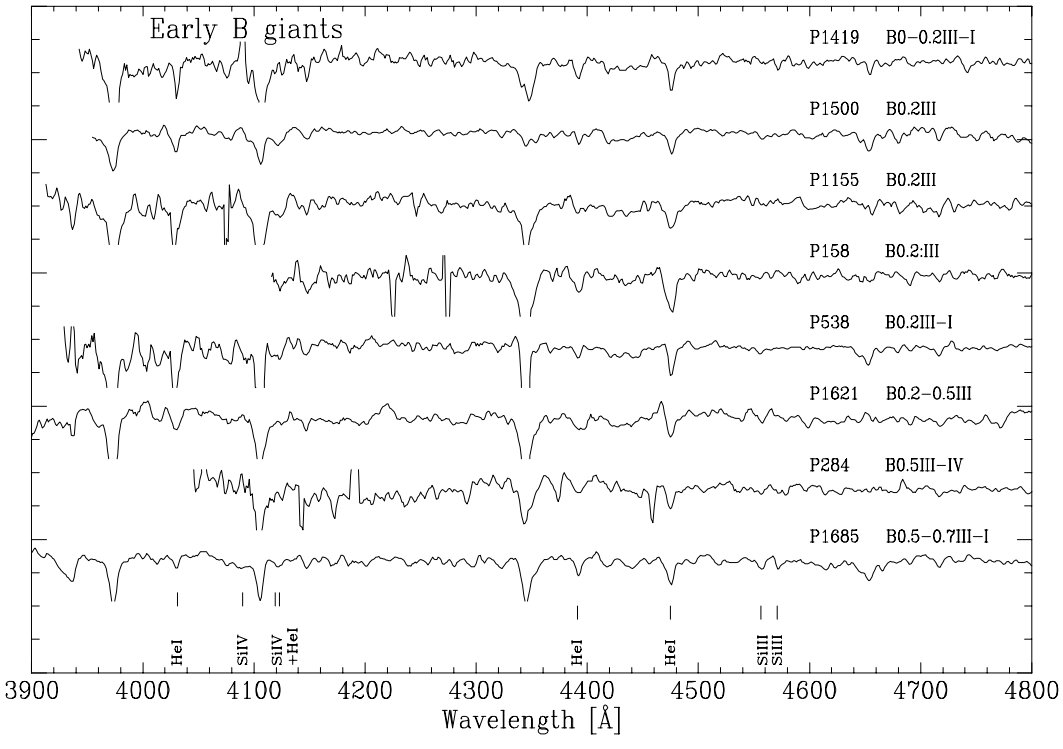

Fig. 21. Same as Fig. 20 for early B-type giant stars

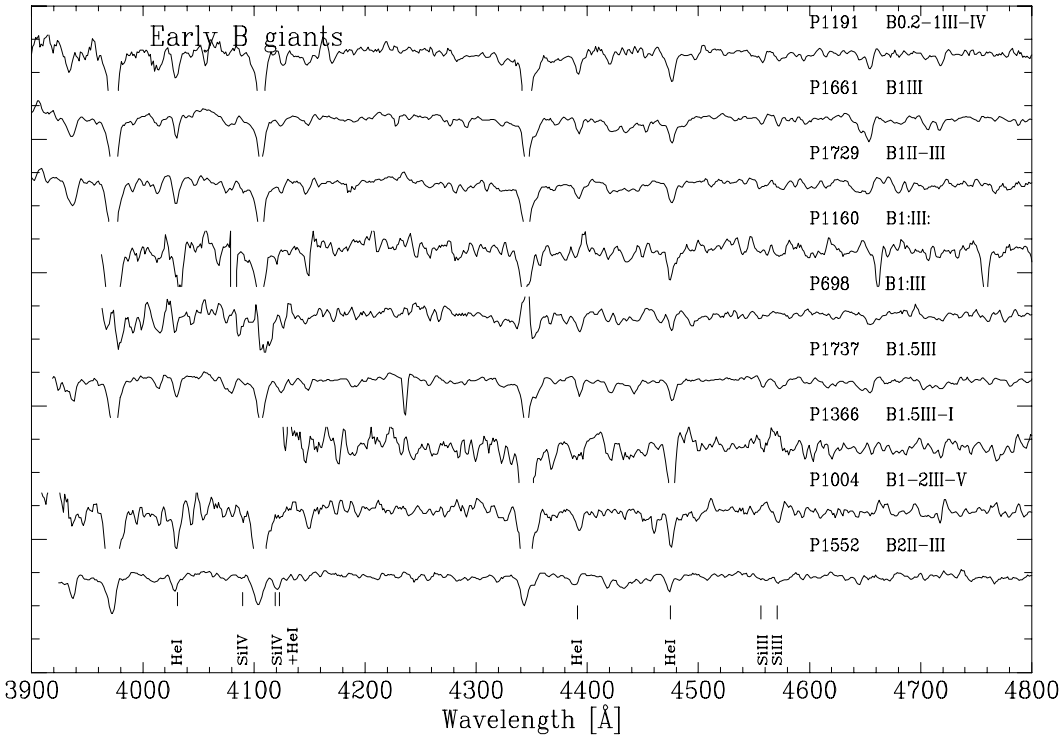

Fig. 22. Same as Fig. 20

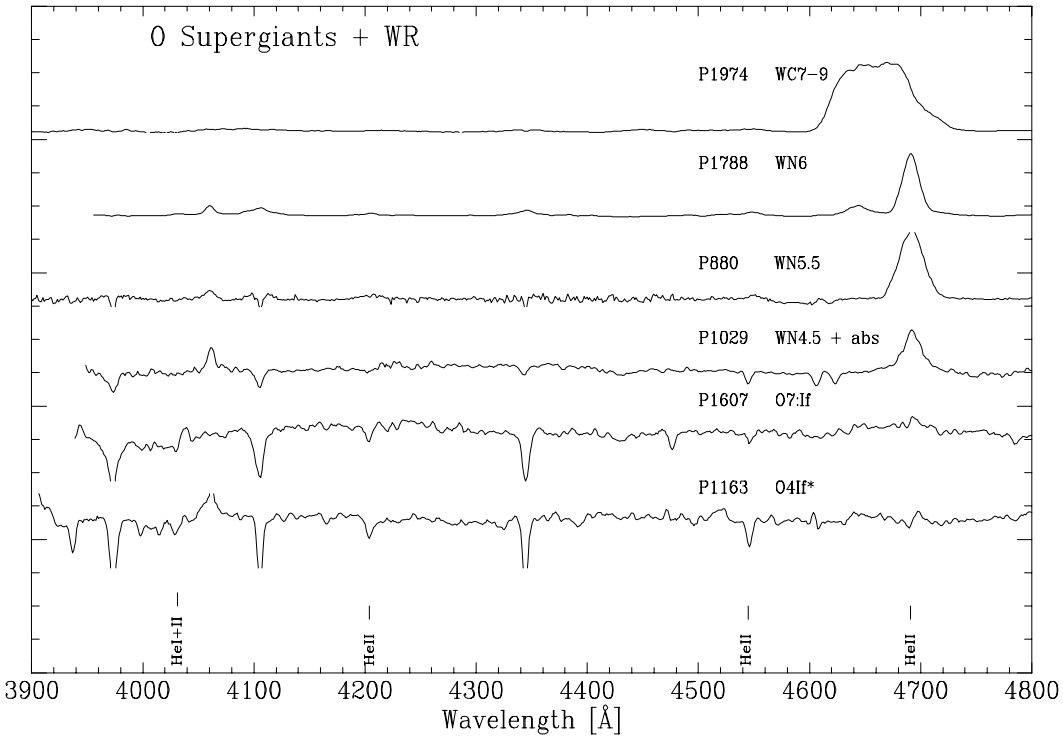

Fig. 23. Spectral classification for O giant and Wolf-Rayet stars

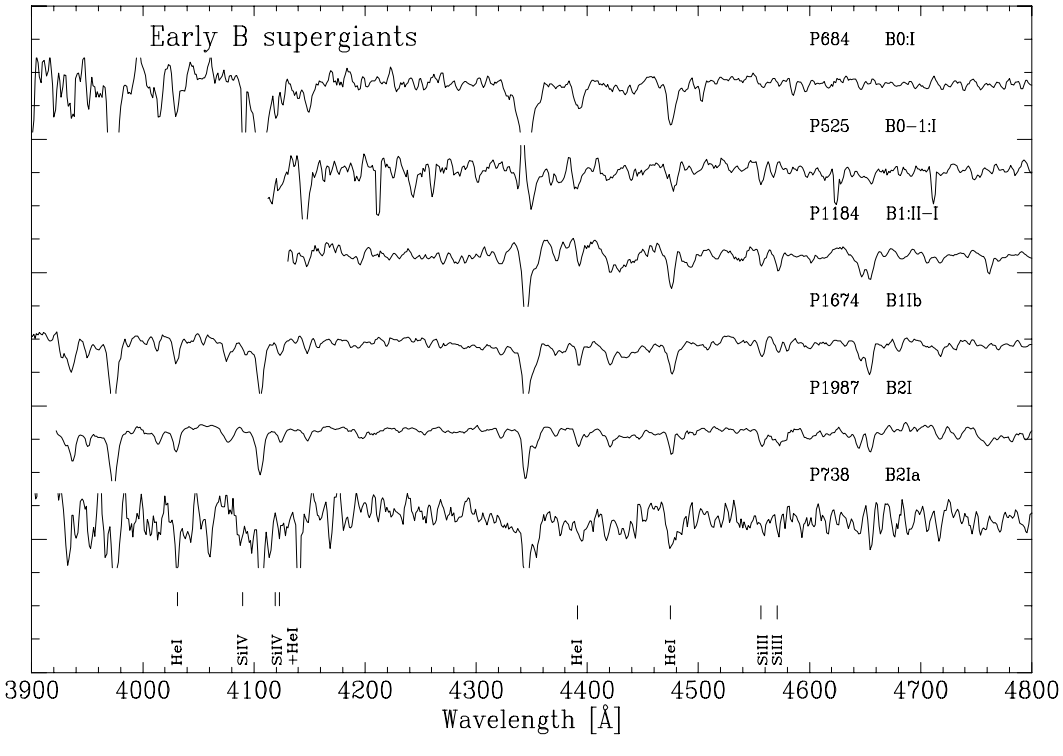

Fig. 24. Spectral classification of B supergiant stars

in order to enhance the weaker features relevant to the classification process.

The resulting spectral types are presented in Table 1. The stellar identifications in Col. 1 are those by Parker (1993) (with the exception of a few stars which lie beyond the area covered by his photometry, namely stars 10001 to 10008). Column 2 shows the visual magnitude from Paper I when available and Parker (1993). The ones from the latter are indicated with a "⋆" symbol. The discrepancies between both photometries has already been discussed in Paper I. Column 3 lists our spectral classification, and Col. 4 indicates previous classification taken mostly from the compilation of Walborn & Blades (1997) (hereafter WB). Table 2 lists the spectral types available in the literature, for stars not observed by us but which have been included in our analysis.

A finding chart for our objects is included in Figs. 1 and 2, where slits have been drawn to scale, showing the corresponding identification number.

4.2. Comparison with other spectral classifications

4.2.1. Ground based data

There are 70 stars in our sample with published spectral types, mostly from WB. A comparison plot of both classifications is presented in Fig. 25, where we plot the spectral types from the literature against our own spectral types. The bars indicate the uncertainty in the spectral classification using the following convention: an O3-6 star appears in the Fig. 25 as an O4.5 type with a ±1.5 error bar in spectral class. From the plot it can be seen that:

1. There is an excellent overall agreement between our spectral types and the ones already published.
2. The "flat" distribution of points in the early-mid O range is mostly due to a number of stars classified as "O3-6V" in WB due to strong nebular contamination, and which we have been able to classify more accurately.
3. We seem to classify late O-type and B-type stars with slightly later types, although the agreement is still quite remarkable.
4. There are 9 stars that fall well away from the diagonal line. These stars are labelled in the diagram and are discussed below.

Our O-type classification was done using better quality data than the previous observations. The improvement comes mostly from our method for subtraction of nebular contamination, and also from a better S/N ratio. However, for the B-type stars the classification is more sensible to spectral resolution, which is slightly better in WB, than to S/N. These facts are relevant in the following discussion of the 9 discrepant cases.

Parker 706: Previously classified as O3V. The spectrum presents HeI absorption lines which indicate a later type (O6V). The residual of the [OIII]5007 Å line is smaller than 4%, which indicates that the chance of HeI being due to over-subtraction is small.

Parker 1013: This star was classified as O8:V by WB, but our data shows no strong HeI absorption features. The nebular spectrum extracted close to the star indicates low probability of HeI under-subtraction. Thus, our O4V type appears more secure.

Parker 547: WB give O8-9V for this star, but our data shows no strong HeI features, although with some uncertainty because the nebular contribution had a high residual before the correction. However, the nebular scaling correction did not change our initial O6V spectral type which we retain.

Parker 1247: We detect a faint HeII 4686 Å feature together with SiIV 4089 – 4116 and SiIII 4552 – 4567. The presence of HeII is not expected in a B2-3 star, as classified in WB, so our B0.5IV type appears more secure.

Parker 1553: This is one of the clearest cases in which there is no HeI emission detected in the background, so the undoubtedly stellar absorption line HeI 4471 makes it an O7V type star.

Parker 1797: The long error bar shows our uncertainty when classifying this star. Notice, however, that according to our estimated contribution of nebular Balmer lines, the hydrogen emission lines seen in the spectrum are intrinsic to this star, so we classify it as Be.

4.2.2. HST data

There are six stars in common with the work of Massey & Hunter (1998) where they present spectral types for stars within the core of the cluster obtained using the Faint Object Spectrograph (FOS) (numbers 860, 863, 1029, 1036, 1080, 1350 in Table 1; plotted in triangles in Fig. 25.) The FOS observations were obtained through a 0.26″ diameter aperture which reduces the nebular contamination considerably, making it negligible for H and HeI lines. From the ratio of slit areas we estimate that the nebular contamination in the FOS spectra is about 40 times smaller than in our NTT observations. On the other hand, there is a big difference in the light collecting areas so, since the exposure times are slightly larger for the NTT data, the overall S/N ratio is significantly larger in our data. Furthermore, the Digicon detector of the FOS is known to introduce problems due to "dead" and noisy diodes. The observational procedure, described by MH, shifts the spectra along 5 neighbouring diodes at a step of 1/4 diode, which means that a diode turned off

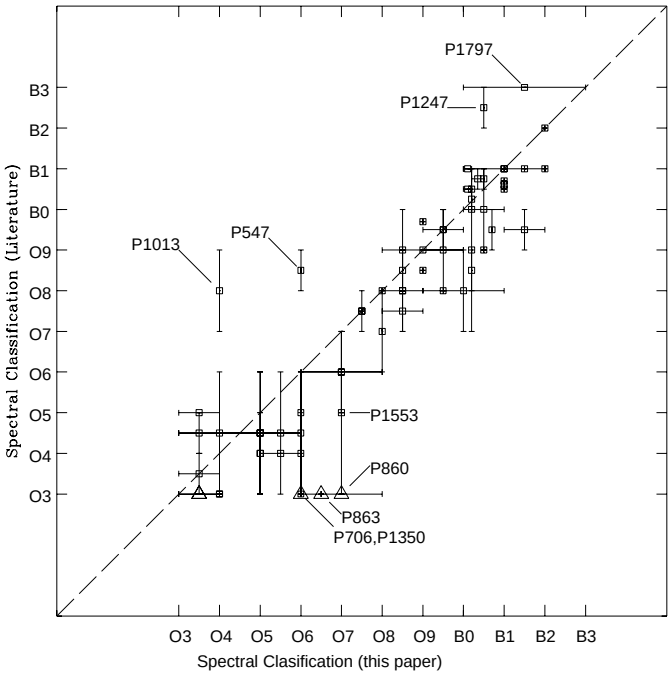

Fig. 25. Comparison between spectral classification described in this paper, and the one found in the literature. Square markers identify the comparison with Walborn & Blades (1997) (WB97) and Parker (1993). Triangle markers indicate the comparison with spectral types in MH. Labelled points are discussed in the text

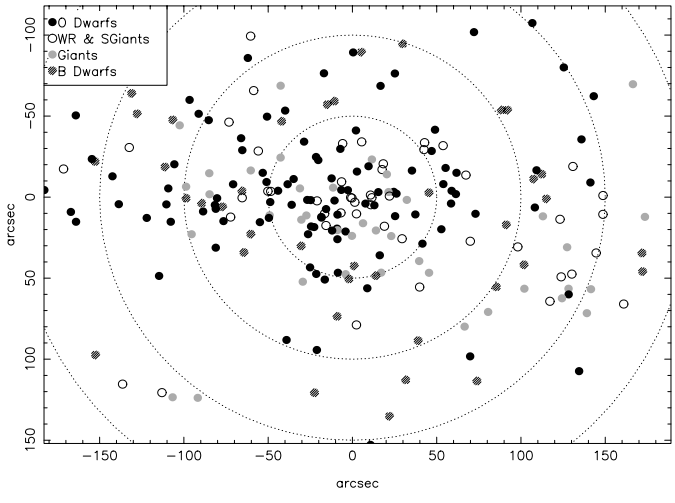

Fig. 26. Spatial distribution of stars classified in this paper. The different distribution of early and late type stars can be seen in this diagram. Coordinates are in arcsec, measured from R136. The dotted circles indicate radial distances from R136, at 50 arcsec steps

reduces the S/N ratio by a factor of $\sim 20\%$, while a noisy diode introduces spurious emission or absorption features that are 20 pixels wide. In particular, at the redshift of 30 Doradus, the HeI 4471 feature lies approximately in diode # 408. According to the information available in the FOS manual, diode # 409 is turned off and diode # 410 is reported as possibly noisy, though still turned on. This reduces considerably the S/N ratio in this region of the spectrum, which unfortunately makes the detection of weak HeI 4471 features rather difficult.

By comparing the FOS intensities of the Hδ and Hγ absorption lines, which are free from nebular contamination in the FOS data, with our NTT data, we can obtain an independent check of the goodness of our nebular subtraction method. Below we present the result of this comparison for the 3 stars for which we disagree with the classification of MH.

Parker 860 (=MH 28) We classify this star as O7:V((f)) although the [OIII] residuals indicate significant nebular contamination of the HeI lines. Comparison of the Balmer lines with the FOS data yield the same estimate, but we still consider that there is real HeI absorption in the spectrum, so the type O3V given by MH is probably not correct.

Parker 863 (=MH 29) We classify this star as O6.5V. Comparison of the Balmer lines in the FOS spectrum indicates that our nebular subtraction is good. Moreover, in this particular case we have detected the stellar HeI 4471 absorption even *without* background subtraction. So again the O3V type given by MH is probably incorrect.

Parker 1350 (=MH H96-28) We classify this star as O6III(f*) while MH give O3III(f*). The presence of NIV 4058 Å emission in the FOS spectra favours the classification of MH, but this feature is probably of instrumental origin. Although there is no report of problems in that area of the detector, the NIV emission feature is 20 pixels wide, matching the extension of a noisy diode feature. Moreover, the NIV feature is not detected in our higher S/N spectrum of the star.

5. Spatial distribution

In Paper I we detected evidence for mass segregation in the 30 Dor cluster. To further investigate this important point we have combined our spectral classification, with that available in the literature, to obtain a total of 235 stars with reliable spectral types within the 30 Dor cluster. This allows us to examine the spatial distribution of stars, grouping them in spectral class bands. The result is shown in Fig. 26 where we have split the stars in four main groups: O dwarfs, B dwarfs, OB giants and OB supergiants (including Wolf-Rayet stars).

It was pointed out by Underhill (1983) that determination of evolutionary stages from spectral types is unreliable. Still there are some clear points that come out of the distribution:

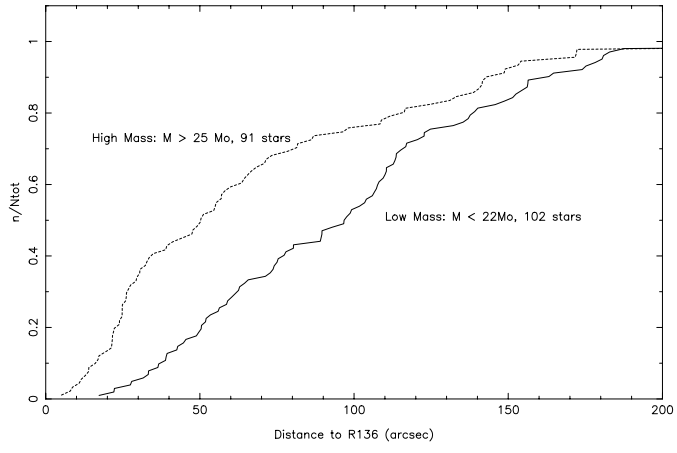

Fig. 27. Cumulative radial distribution of stars according to masses determined from their spectral types. Both distributions are plotted with dashed and continuous line styles, for the high-mass and low-mass stars respectively. The different distribution for both subsets indicates the presence of mass segregation

1. Giant and supergiant stars are evenly distributed in the sampled region (our sample is intrinsically stretched in the N-S direction).
2. O dwarfs are notoriously concentrated towards R136.
3. There is a large region, south-east of R136, where the number of late type stars is much larger than that of early type ones. These stars can be identified in the center of Fig. 2.

We have also estimated the stellar masses of stars from their spectral types interpolating from the relationship tabulated by Schmidt-Kaler (1982). With these values we analysed the radial distribution of stars according to their masses. As the determination of a star's mass from it's spectral type is not very accurate, we split the dataset in two large groups: high mass and low mass stars, with the transition at $\sim 23.5\,M_{\odot}$. Figure 27 shows the cumulative distribution of stars from the centre of the cluster. It can be readily seen that the massive stars show a concentrated distribution, while the lower mass stars have a flatter distribution, with few stars in the inner region. Thus, there is evidence for mass segregation in the 30Dor cluster, as it is also suggested from the photometric analysis of Paper I. A Kolmogorov-Smirnov test to both distributions, yields a significance level of 0.007, which indicates that the distribution of high mass stars is significantly different from the less massive ones.

In previous works, Malumuth & Heap (1994) and Brandl et al. (1996) had also found mass segregation in the inner region of 30Dor, close to R136, which agrees with our findings. Malumuth & Heap detected a difference in the slope of the IMF of stars within a 3.3 arcsec radius of R136a and of those outside this area. Brandl et al. detected changes in the IMF slope and a clear trend towards smaller core radii for brighter –more massive– stars. Thus, there is evidence for mass segregation at the core and outer regions of 30 Dor. We believe that these results are also compatible with the lack of change of the IMF slope found by Hunter et al. (1996) given the narrow mass range and the restricted radial range of their data.

A more detailed analysis of this important point will be discussed in Paper III where we combine the masses derived from our photometric and spectroscopic observations.

6. Summary

We have obtained 175 spectral types for stars in 30 Doradus of which 105 are new. The total number of stars with spectral classification is now 261, which allows a thorough spectrophotometric analysis of the region. We have used the [OIII] nebular lines to reduce the contamination effects of the ionised nebula to the stellar spectra, improving the reliability of the spectral classification from ground based spectroscopy. Our spectral classification is good to about ± 1.2 subtypes. The spatial distribution of spectral types suggests the presence of a later type group $2'$ south of R136. The radial distribution of stars according to the masses estimated from their spectral types shows a more compact distribution for the most massive stars, indicating the existence of mass segregation in the cluster.

References

Brandl B., Sams B.J., Bertoldi F., et al., 1996, ApJ 466, 254
Ellis R.S., 1997, ARA&A 35, 389
Elmegreen B.G., 1997, ApJ 486, 944
Hunter D.A., O'Neil E.J., Lynds R., et al., 1996, ApJ 459, L27
Malumuth E.M., Heap S.E., 1994, AJ 107, 1054
Massey P., 1985, PASP 97, 5
Massey P., 1998, in Stellar Astrophysics for the Local Group, Aparicio A., Herrero A. and Sánchez F. (eds.). Cambridge University Press, Cambridge, UK
Massey P., Hunter D.A., 1998, ApJ 493, 180 (MH)
Melnick J., 1985, A&A 153, 235
Parker J.Wm., 1993, AJ 106, 560
Schmidt-Kaler Th., 1982, in Stars and Star Clusters, Vol. 2b, Schaifers K. and Voigt H.H. (eds.), part of the Landolt-Börstein series on Numerical Data & Functional Relationships in Science and Technology. Springer-Verlag, Berlin-Heidelberg
Selman F.J., Melnick J., Bosch G.L., Terlevich R.J., 1999, A&A 341, 98 (Paper I)
Stasinska G., Leitherer C., 1996, ApJS 107, 661
Underhill A.B., 1983, in: Garrison R.F. (ed.), The MK Process and Stellar Classification. David Dunlap Observatory, Toronto, p. 60
Walborn N.R., 1991, in: Haynes R., Milne D. (eds.), IAU Symp. 148, The Magellanic Clouds. Kluwer, Dordrecht, p. 145
Walborn N.R., Blades J.C., 1997, ApJSS 112, 457
Walborn N.R., Fitzpatrick E.L., 1990, PASP 102, 379